Electronic Supplementary Material (ESI) for Journal of Materials Chemistry B.

Revealing the role of different nitrogen functionalities on the drug delivery performance of graphene quantum dots: A combined density functional theory and molecular dynamics approach

Morteza Vatanparast, Zahra Shariatinia*

Department of Chemistry, Amirkabir University of Technology (Tehran Polytechnic),

P.O.Box:15875-4413, Tehran, Iran.

* Corresponding author. Tel.: +982164545810.
E-mail address: shariati@aut.ac.ir

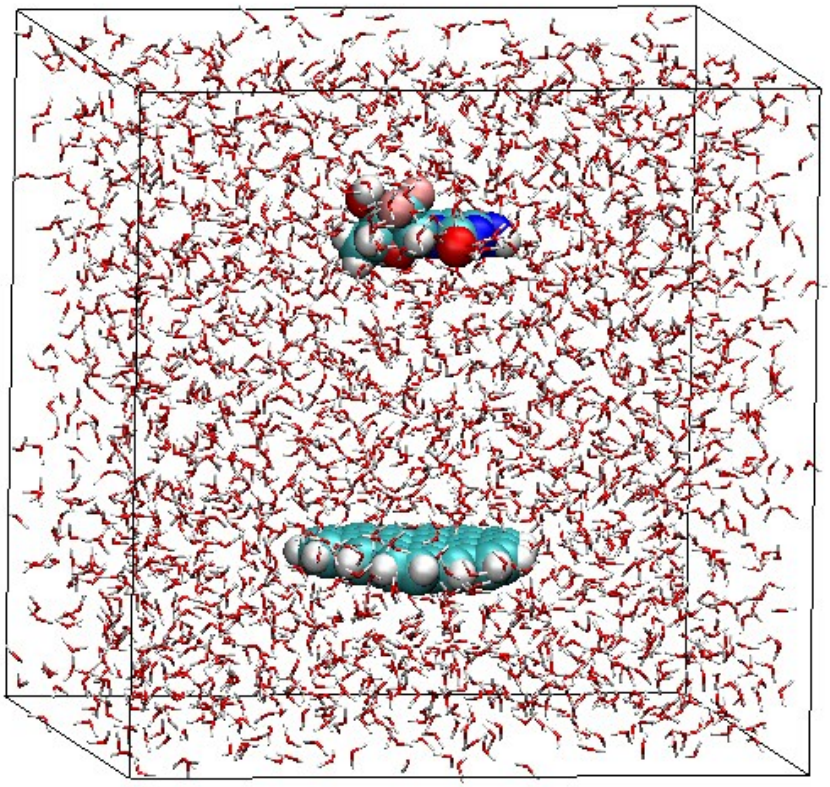

Fig. S1. A schematic of the simulation box for the penetration of the drug-loaded nanocarriers across the cell membrane

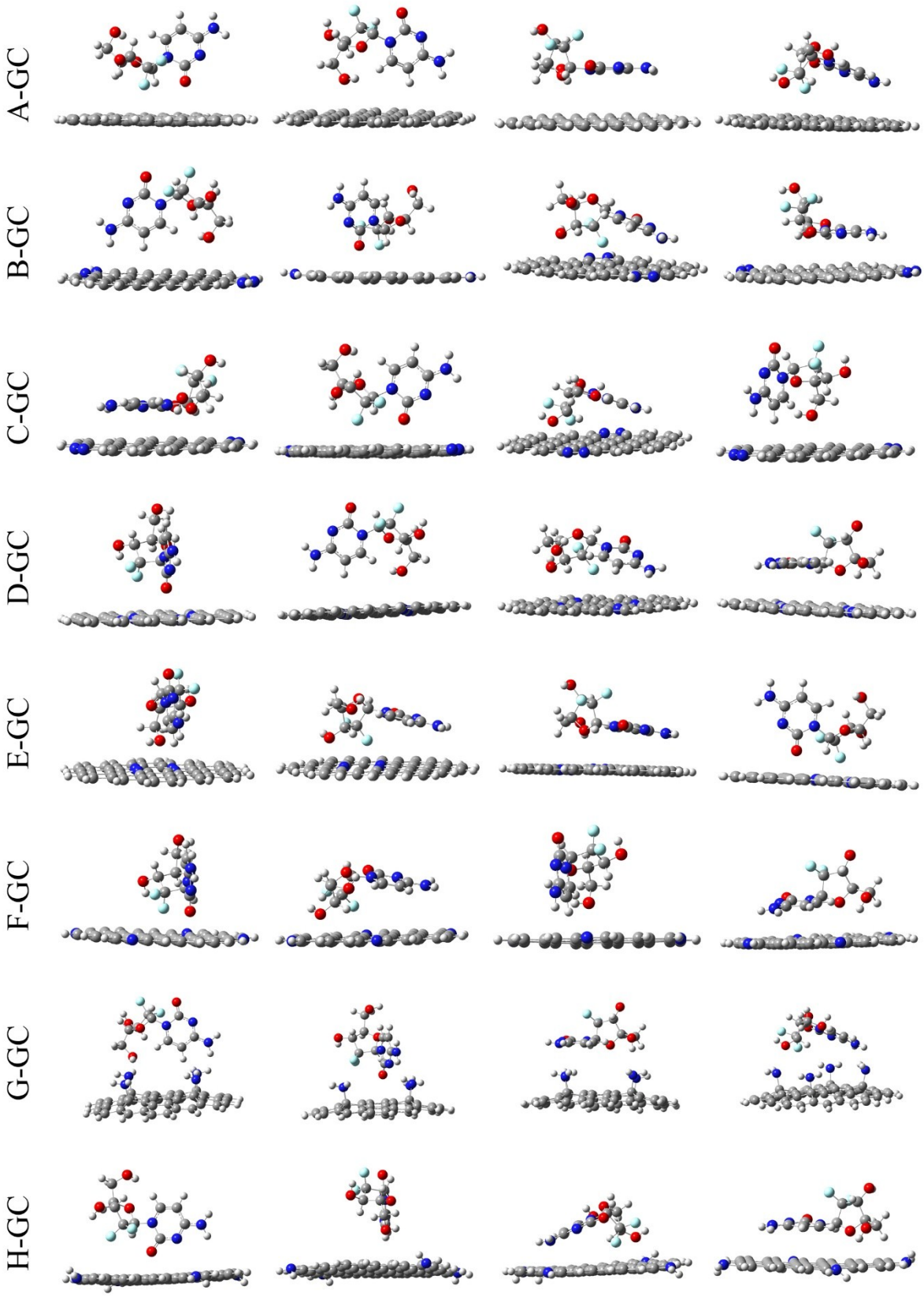

Fig. S2. Some initial structures for the adsorption of GC drug on the nanocarriers surfaces.

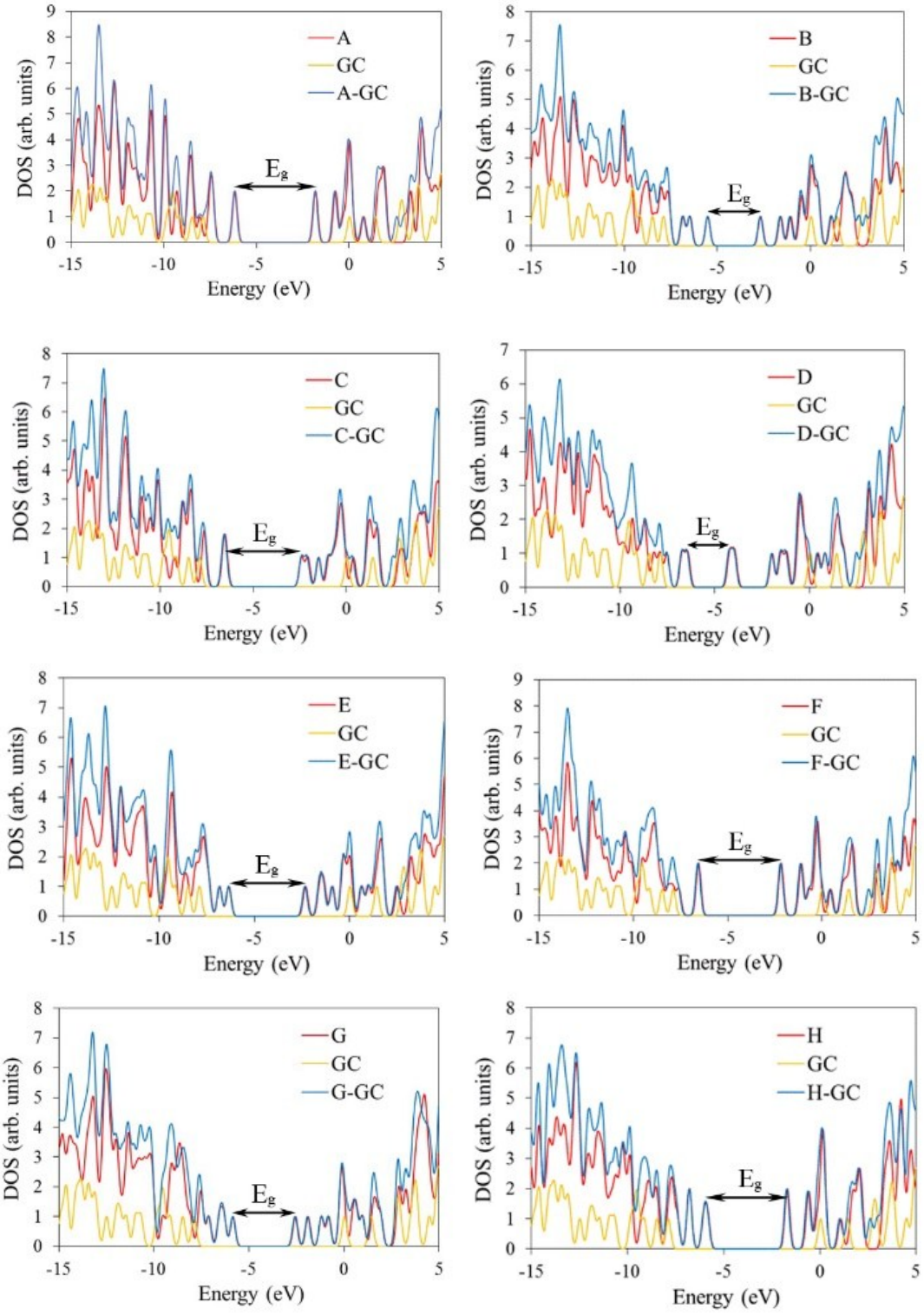

Fig. S3. The density of states (DOS) plots for the BN nanosheet, GC drug, nanocarriers and their complexes.

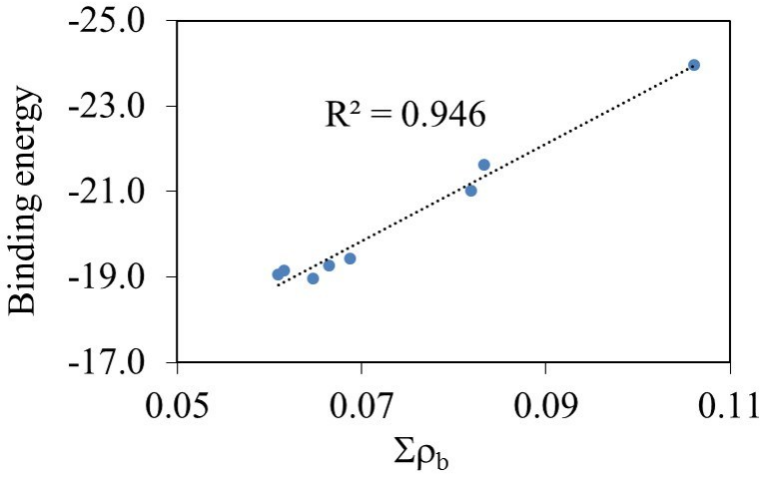

Fig. S4. Correlation between binding energy (kcal mol^{-1}) and sum of electron density ($\Sigma\rho_b$).

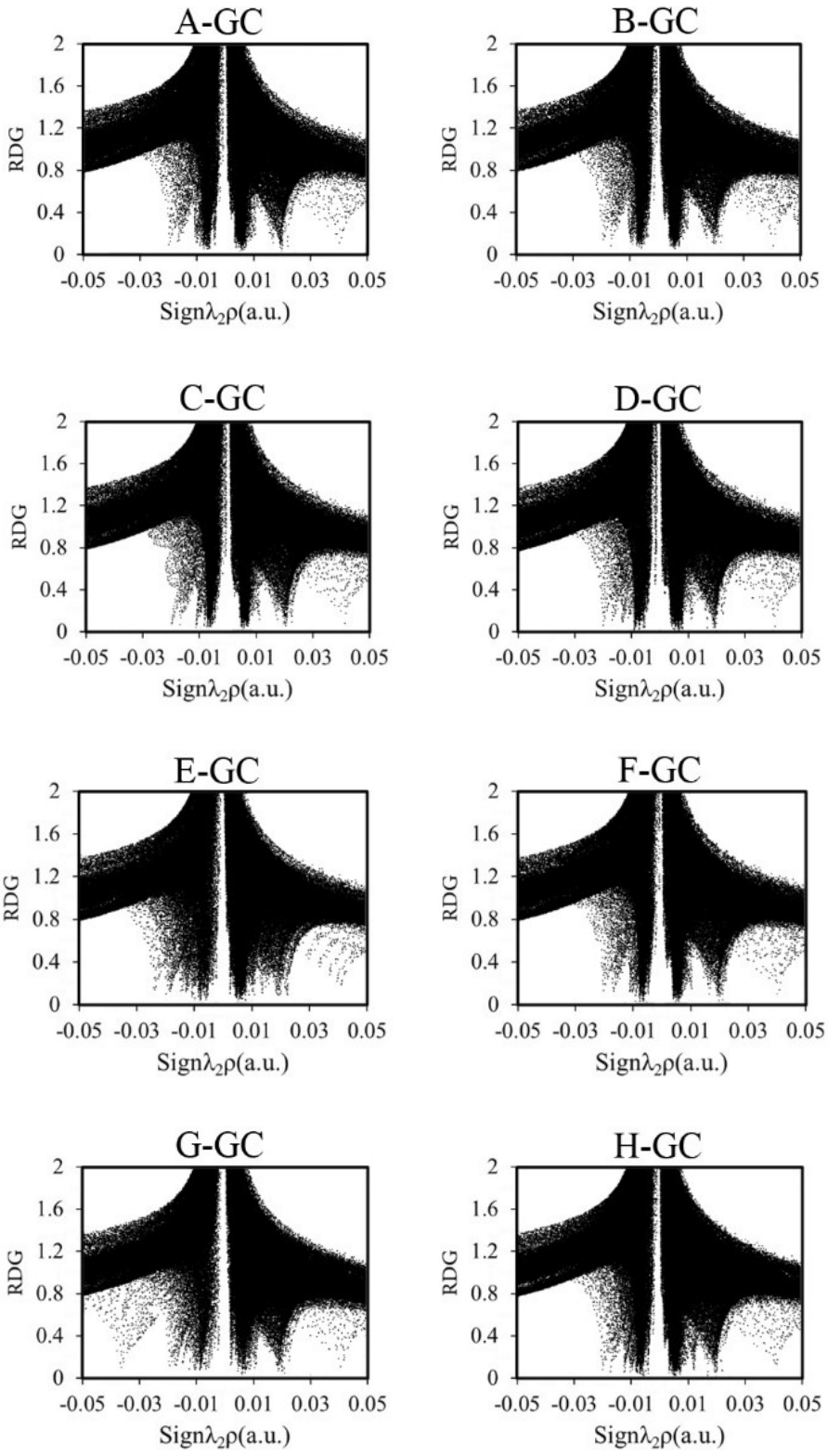

Fig. S5. The scatter plot of RDG versus sign(λ_2)ρ for the studied systems.

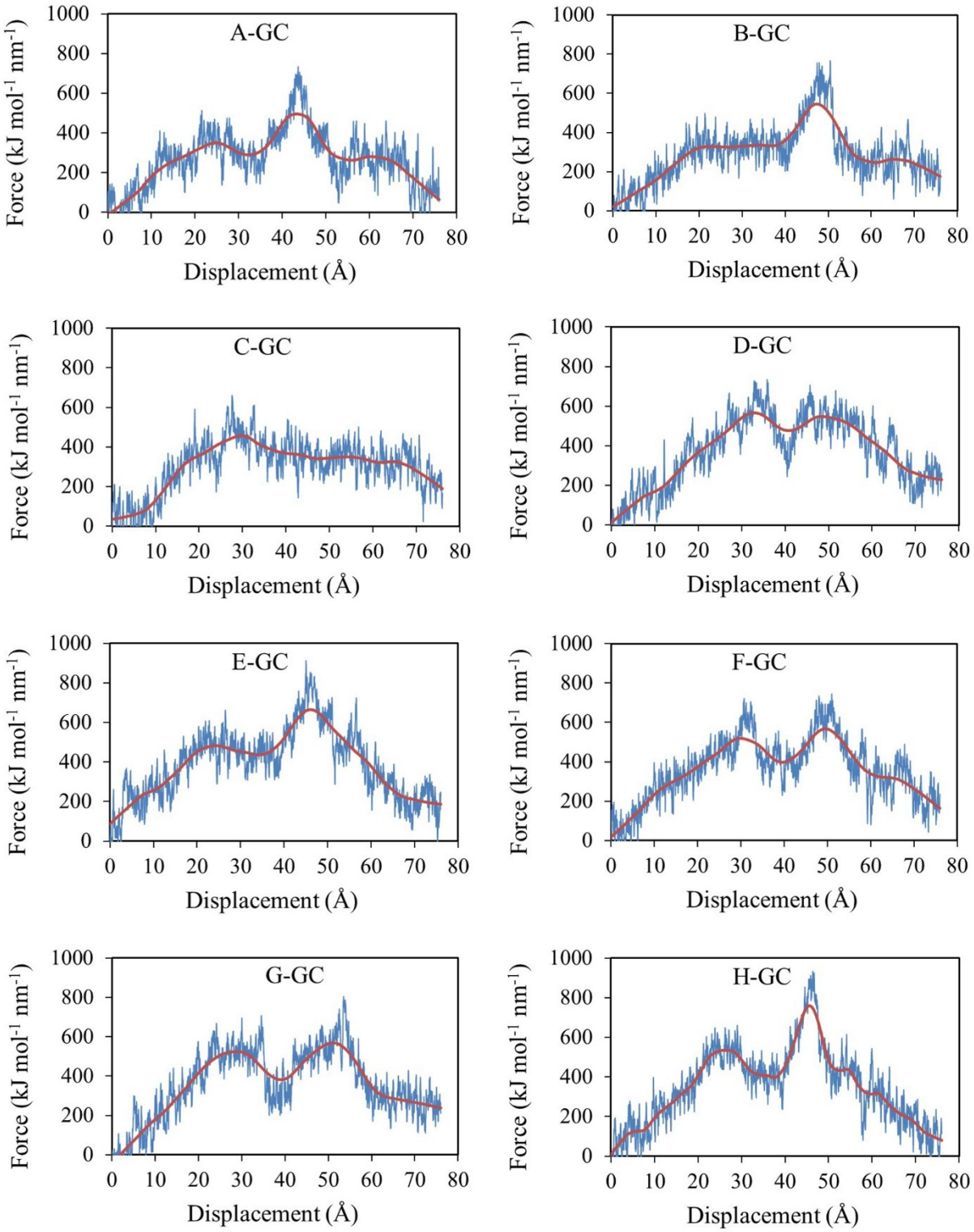

Fig. S6. The force-displacement profiles of drug-loaded nanocarriers during the penetration for obliquely orientations.

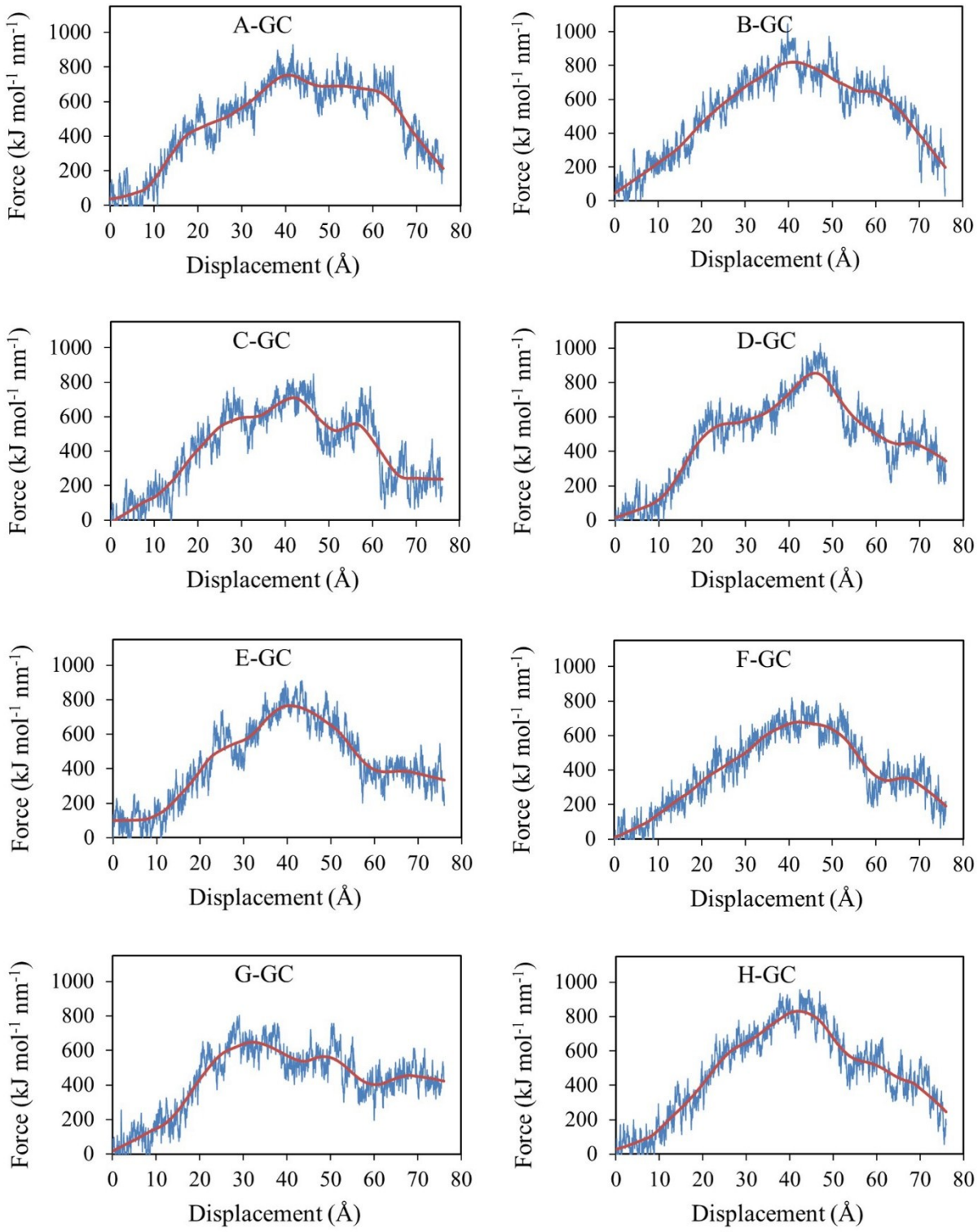

Fig. S7. The force-displacement profiles of drug-loaded nanocarriers during the penetration for parallel orientations.

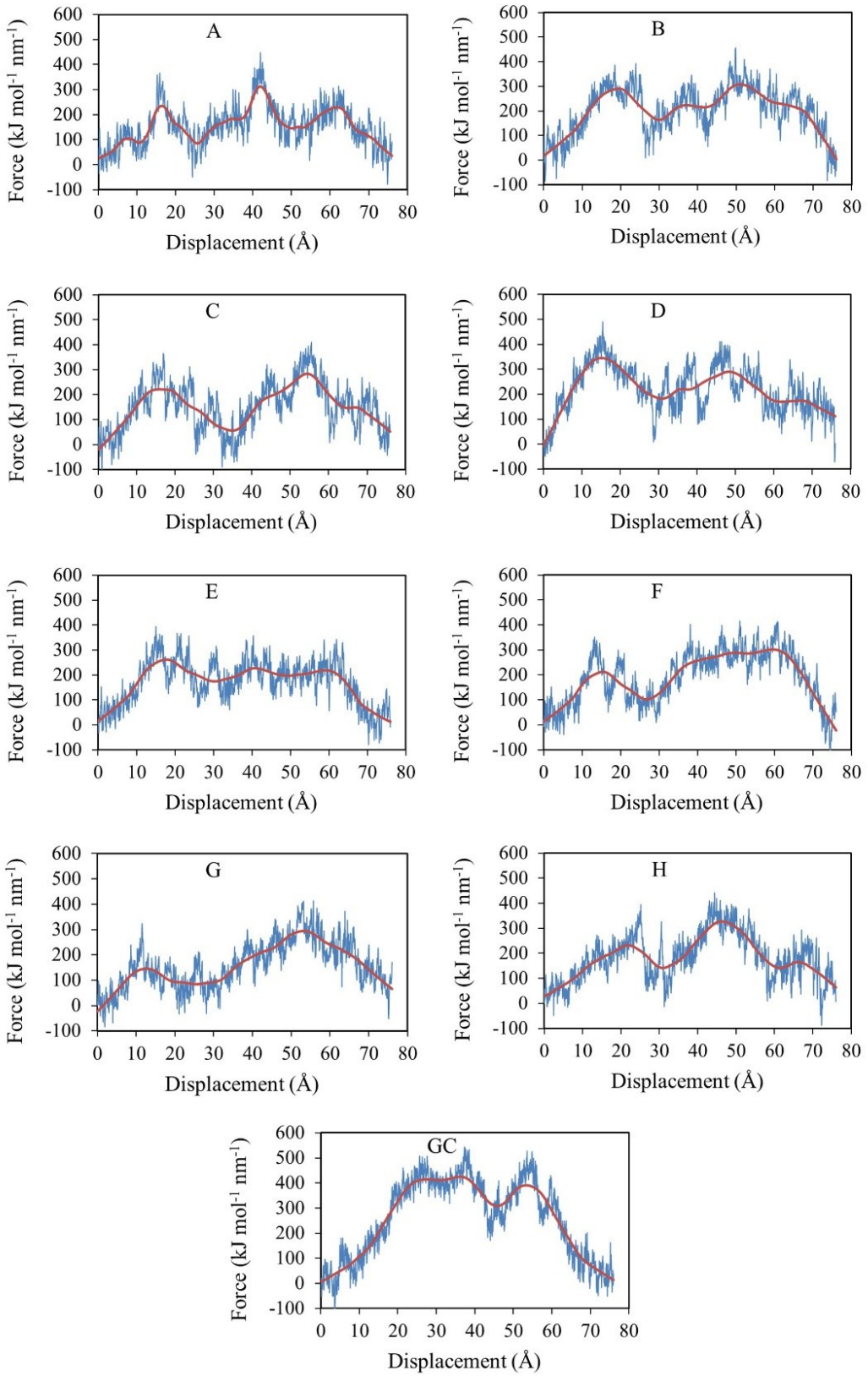

Fig. S8. The force-displacement profiles of GC drug and nanocarriers during the penetration for the perpendicular orientations (structures labelled with A, B, C, D, E, F, G and H are introduced in Fig. 2).

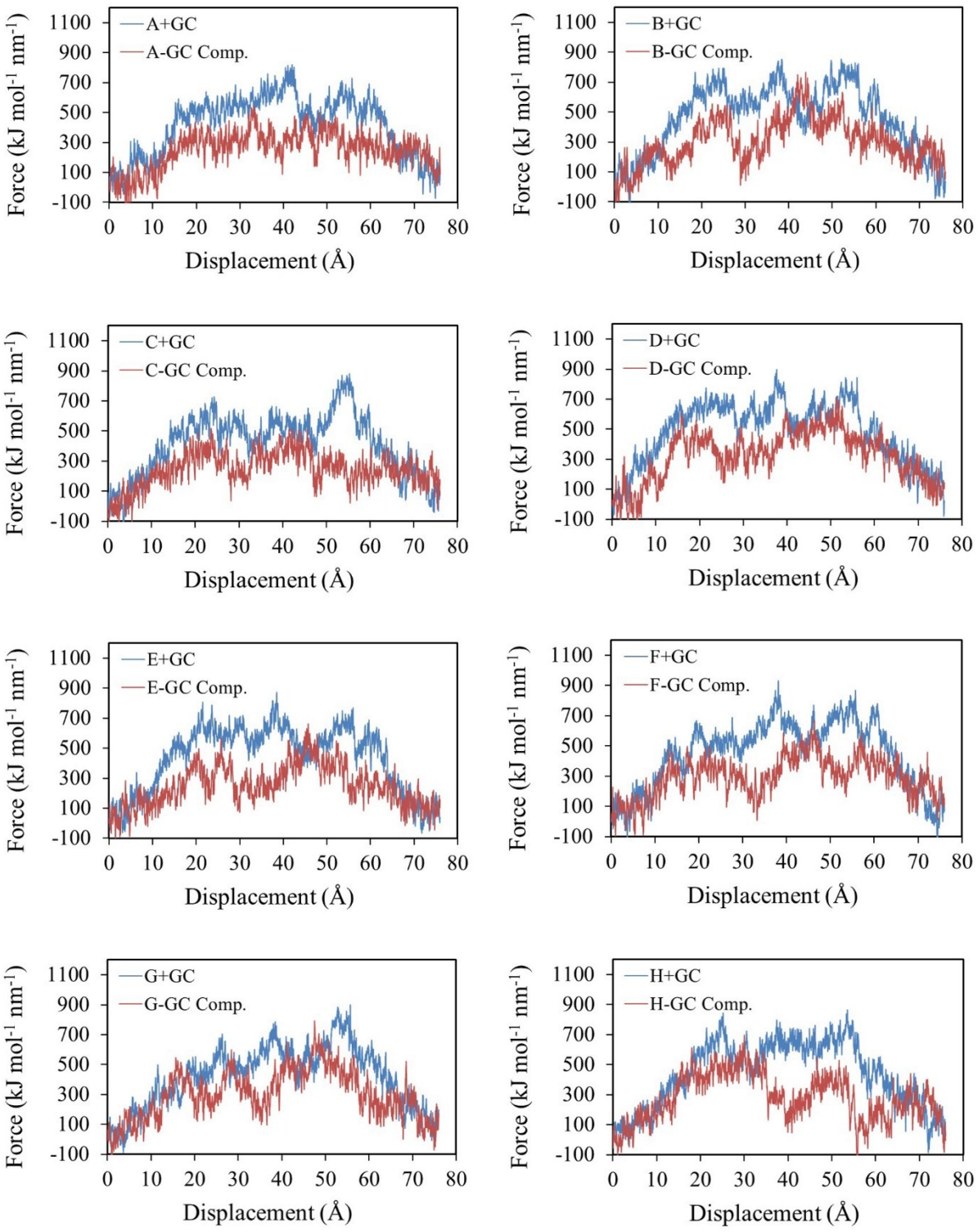

Fig. S9. The force-displacement profiles of the nanocarrier-GC complexes and the sum of the monomers during the penetration for perpendicular orientations.

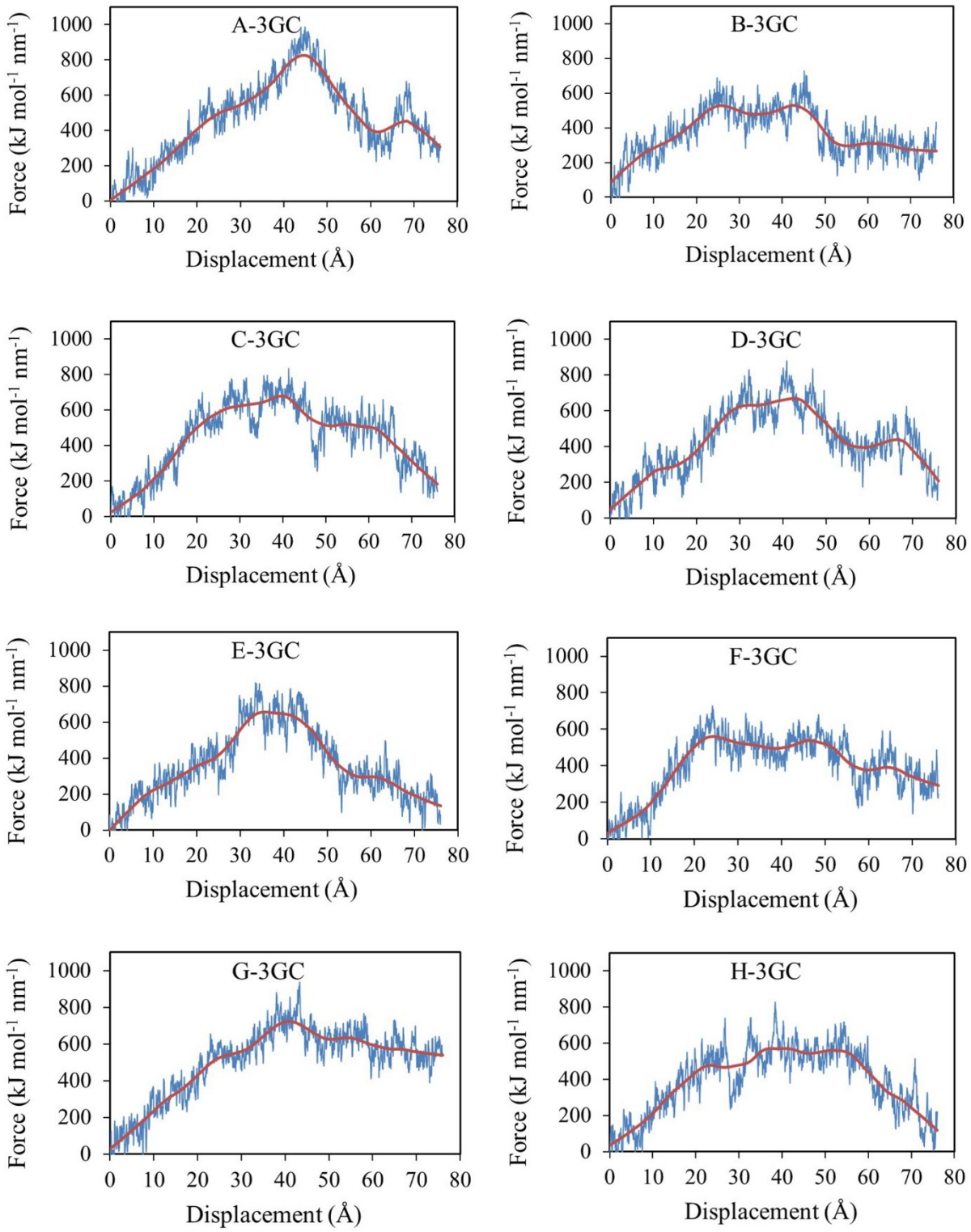

Fig. S10. The force-displacement profiles of GC-nanocarrier (3:1 ratio) complexes during the penetration for perpendicular orientations.

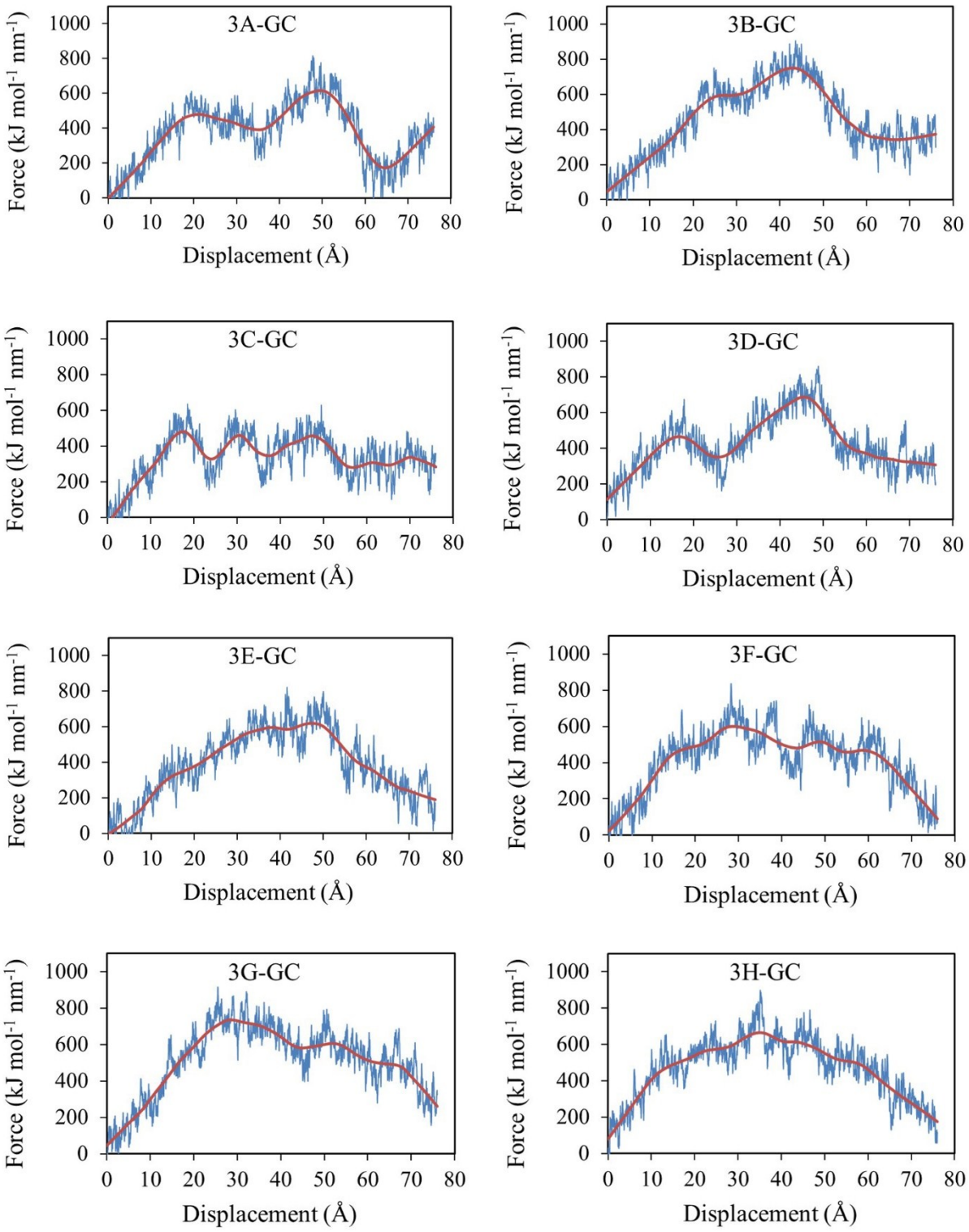

Fig. S11. The force-displacement profiles of GC-nanocarrier (1:3 ratio) complexes during the penetration for perpendicular orientations.

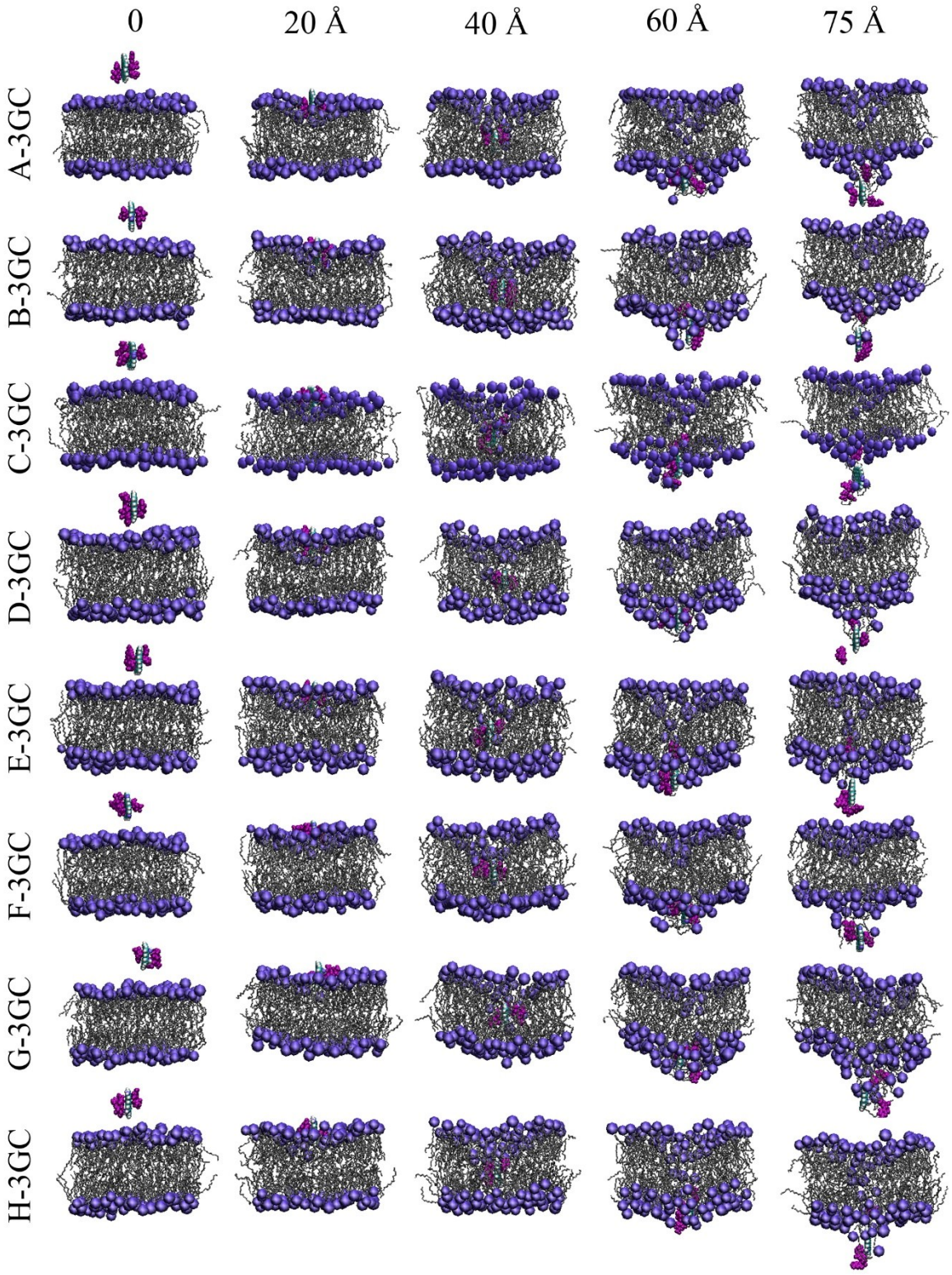

Fig. S12. Snapshots of GC-nanocarrier (3:1 ratio) complexes penetration through the membrane for perpendicular orientation.

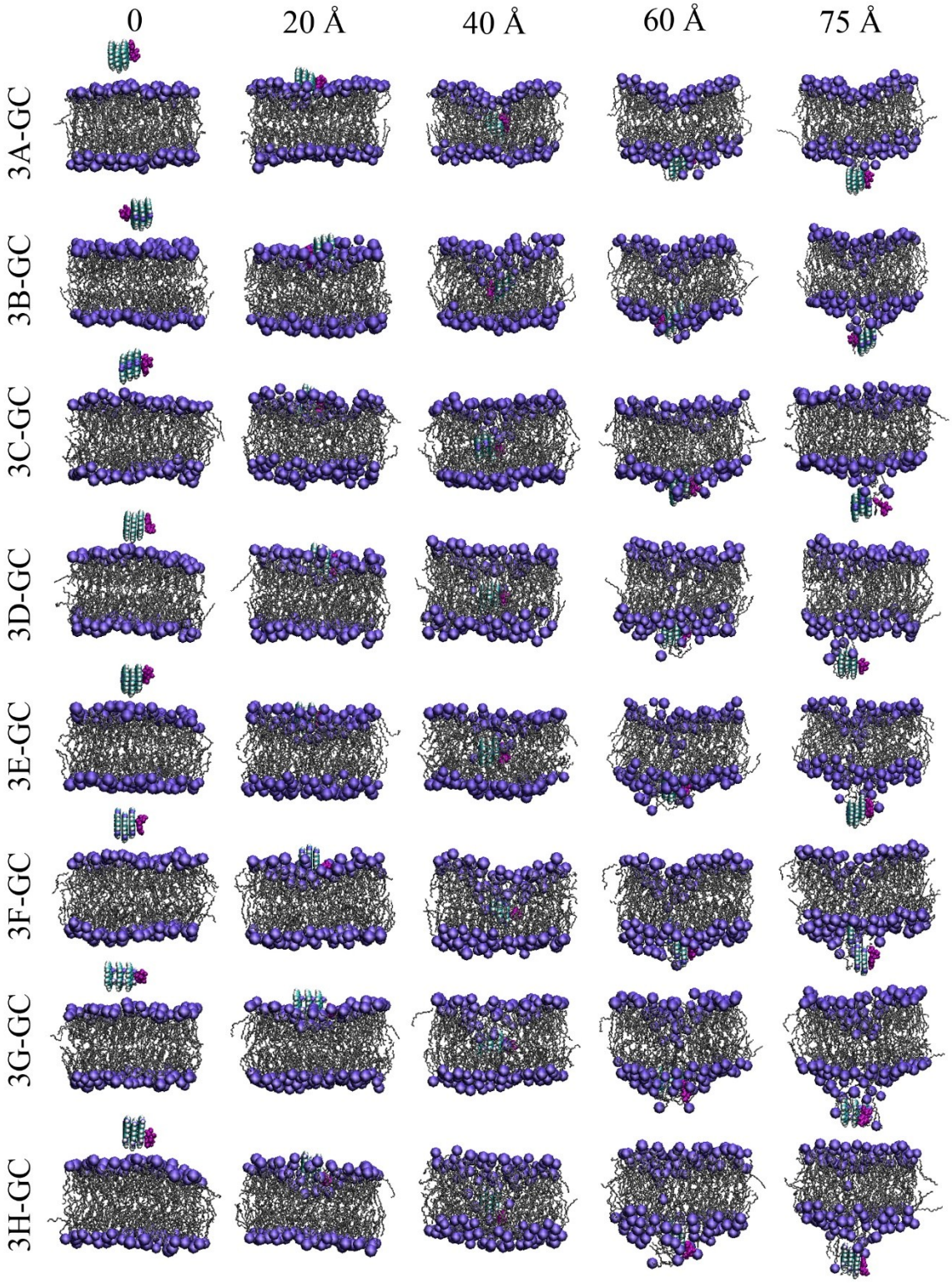

Fig. S13. Snapshots of GC-nanocarrier (1:3 ratio) complexes penetration through the membrane for perpendicular orientation.

Table S1. The electron density (ρ_b), Laplacian of electron density ($\nabla^2\rho_b$), kinetic electron energy density (G_b), potential electron energy density (V_b), total electron energy density (H_b) and $-G_b/V_b$ ratio at the bond critical points (BCPs) of the studied complexes. All the values are in au.

System	No. BCP	ρ_b	$\nabla^2\rho_b$	G_b	V_b	H_b	$-G_b/V_b$
A-GC	1	0.0057	0.0181	0.0039	-0.0032	0.0006	1.1986
	2	0.0056	0.0169	0.0037	-0.0032	0.0005	1.1683
	3	0.0077	0.0267	0.0054	-0.0042	0.0013	1.3015
	4	0.0068	0.0240	0.0048	-0.0035	0.0012	1.3509
	5	0.0080	0.0242	0.0050	-0.0040	0.0010	1.2563
	6	0.0074	0.0270	0.0055	-0.0042	0.0013	1.2972
	7	0.0108	0.0381	0.0086	-0.0076	0.0010	1.1259
	8	0.0090	0.0312	0.0064	-0.0051	0.0014	1.2711
B-GC	1	0.0060	0.0194	0.0041	-0.0033	0.0008	1.2311
	2	0.0059	0.0187	0.0040	-0.0034	0.0007	1.1931
	3	0.0077	0.0271	0.0055	-0.0043	0.0013	1.2950
	4	0.0068	0.0247	0.0049	-0.0036	0.0013	1.3588
	5	0.0074	0.0220	0.0046	-0.0037	0.0009	1.2525
	6	0.0080	0.0291	0.0060	-0.0047	0.0013	1.2752
	7	0.0105	0.0368	0.0083	-0.0074	0.0009	1.1216
	8	0.0093	0.0320	0.0066	-0.0053	0.0014	1.2616
C-GC	1	0.0058	0.0179	0.0039	-0.0032	0.0006	1.1892
	2	0.0065	0.0193	0.0042	-0.0036	0.0006	1.1610
	3	0.0076	0.0266	0.0054	-0.0041	0.0012	1.3001
	4	0.0075	0.0274	0.0055	-0.0041	0.0014	1.3455
	5	0.0074	0.0220	0.0046	-0.0036	0.0009	1.2546
	6	0.0068	0.0246	0.0049	-0.0037	0.0012	1.3360
	7	0.0071	0.0259	0.0052	-0.0040	0.0013	1.3138
	8	0.0114	0.0404	0.0091	-0.0081	0.0010	1.1200
	9	0.0086	0.0300	0.0061	-0.0048	0.0013	1.2816
D-GC	1	0.0070	0.0212	0.0046	-0.0040	0.0007	1.1713
	2	0.0086	0.0262	0.0060	-0.0054	0.0006	1.1051
	3	0.0084	0.0295	0.0065	-0.0056	0.0009	1.1606
	4	0.0089	0.0326	0.0066	-0.0051	0.0015	1.3026
	5	0.0075	0.0215	0.0045	-0.0037	0.0008	1.2256
	6	0.0069	0.0212	0.0048	-0.0042	0.0005	1.1288
	7	0.0071	0.0247	0.0050	-0.0038	0.0012	1.3149
	8	0.0132	0.0472	0.0112	-0.0106	0.0006	1.0585
	9	0.0069	0.0265	0.0053	-0.0040	0.0013	1.3223
	10	0.0087	0.0300	0.0062	-0.0049	0.0013	1.2586

E-G	1	0.0110	0.0409	0.0086	-0.0071	0.0016	1.2256
	2	0.0143	0.0524	0.0121	-0.0112	0.0010	1.0867
	3	0.0099	0.0395	0.0086	-0.0074	0.0012	1.1658
	4	0.0131	0.0470	0.0109	-0.0100	0.0009	1.0889
	5	0.0088	0.0348	0.0076	-0.0065	0.0011	1.1731
	6	0.0131	0.0474	0.0108	-0.0098	0.0010	1.1019
	7	0.0085	0.0279	0.0058	-0.0045	0.0012	1.2704
	8	0.0080	0.0236	0.0050	-0.0041	0.0009	1.2196
	9	0.0059	0.0206	0.0041	-0.0030	0.0011	1.3506
	10	0.0067	0.0206	0.0045	-0.0039	0.0006	1.1512
	11	0.0067	0.0199	0.0044	-0.0039	0.0005	1.1363
F-GC	1	0.0059	0.0184	0.0040	-0.0033	0.0006	1.1855
	2	0.0062	0.0184	0.0041	-0.0035	0.0006	1.1597
	3	0.0077	0.0269	0.0055	-0.0042	0.0013	1.3000
	4	0.0046	0.0177	0.0038	-0.0031	0.0007	1.2140
	5	0.0073	0.0262	0.0052	-0.0039	0.0013	1.3415
	6	0.0076	0.0228	0.0047	-0.0038	0.0010	1.2555
	7	0.0072	0.0263	0.0053	-0.0041	0.0013	1.3076
	8	0.0109	0.0391	0.0088	-0.0078	0.0010	1.1264
	9	0.0090	0.0311	0.0064	-0.0050	0.0014	1.2756
G-GC	1	0.0372	0.0974	0.0273	-0.0302	-0.0029	0.9028
	2	0.0088	0.0290	0.0060	-0.0047	0.0013	1.2654
	3	0.0091	0.0306	0.0066	-0.0056	0.0010	1.1870
	4	0.0151	0.0445	0.0107	-0.0103	0.0004	1.0378
	5	0.0090	0.0320	0.0071	-0.0062	0.0009	1.1489
	6	0.0089	0.0301	0.0061	-0.0048	0.0014	1.2912
	7	0.0128	0.0461	0.0103	-0.0091	0.0012	1.1352
	8	0.0070	0.0344	0.0071	-0.0057	0.0015	1.2606
	9	0.0111	0.0389	0.0085	-0.0074	0.0012	1.1599
	10	0.0174	0.0572	0.0145	-0.0146	-0.0002	0.9880
H-GC	1	0.0057	0.0182	0.0039	-0.0032	0.0007	1.2117
	2	0.0053	0.0163	0.0035	-0.0030	0.0005	1.1698
	3	0.0077	0.0266	0.0054	-0.0042	0.0012	1.2939
	4	0.0038	0.0145	0.0030	-0.0023	0.0006	1.2775
	5	0.0067	0.0234	0.0047	-0.0035	0.0012	1.3449
	6	0.0080	0.0239	0.0050	-0.0040	0.0010	1.2538
	7	0.0076	0.0275	0.0056	-0.0043	0.0013	1.2937
	8	0.0105	0.0372	0.0084	-0.0074	0.0010	1.1300
	9	0.0094	0.0327	0.0068	-0.0054	0.0014	1.2606